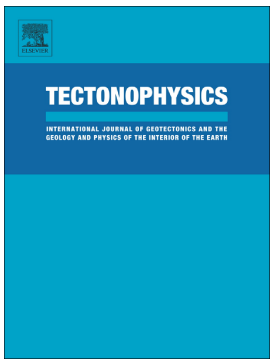

Unraveling the complex deformation pattern at Yellowstone plateau through seismicity and fracture analysis

E. Russo, A. Tibaldi, G.P. Waite, F.L. Bonali, F. Massin, J. Farrell

PII: S0040-1951(20)30035-4

DOI: https://doi.org/10.1016/j.tecto.2020.228352

Reference: TECTO 228352

To appear in: *Tectonophysics*

Received date: 17 October 2019

Revised date: 23 January 2020

Accepted date: 26 January 2020

Please cite this article as: E. Russo, A. Tibaldi, G.P. Waite, et al., Unraveling the complex deformation pattern at Yellowstone plateau through seismicity and fracture analysis, *Tectonophysics*(2018), https://doi.org/10.1016/j.tecto.2020.228352

Unraveling the complex deformation pattern at Yellowstone plateau through seismicity and fracture analysis

Russo E.[1,2*], *Tibaldi A.*[1,2], *Waite G.P.*[3], *Bonali F.L.*[1,2], *Massin F.*[4], *Farrell J.*[5]
[1] *Department of Earth and Environmental Sciences, University of Milan-Bicocca, Milan, Italy*
[2] *CRUST- Interuniversity Center for 3D Seismotectonics with Territorial Applications, Italy*
[3] *Department of Geological and Mining Engineering and Science, Michigan Technological University, Houghton, USA*
[4] *ETH-Zurich, Swiss Seismological Service (SED), CH-8092 ETH-Zurich, Switzerland*
[5] *Department of Geology and Geophysics, University of Utah, Salt Lake City, Utah, USA*

[*]*Corresponding author: Dr. Elena Russo, Department of Earth and Environmental Sciences, University of Milan-Bicocca, P. della Scienza 4, 20126-Milan, Italy; e-mail e.russo11@campus.unimib.it, tel. +39 0264482066*

Abstract

The intense unrest of the Yellowstone volcanic plateau is manifested through diffuse seismic activity, earthquake swarms, and episodes of complex surficial deformation that have been related to magmatic fluid transfer in the upper crust over the past several decades. While past studies have focused on modeling contemporary geophysical data, there has not been a fully-integrated evaluation of seismicity, fault kinematics, and stress field. Here we analyze a catalog of 10,201 relocated earthquakes recorded between 2010 and 2016 and determine 224 well-constrained double-couple focal mechanisms. The majority of the focal mechanisms (65%) are associated with the 2010 Madison Plateau seismic swarm. The focal mechanisms are predominantly strike-slip with subordinate normal faulting mechanisms. Possible causes of this predominance and of the concurrence of both kinematics are here discussed, in order to unravel the influence of magmatic processes such as past sill intrusions. The earthquake catalog has been analyzed in terms of location, time, and kinematics according to the phases of surficial deformation documented by GPS data in order to identify systematic patterns of deformation and has been compared to the 1988-2009 seismicity. The continuous downwarping of the overburden from 2010-2016 was accomodated by structural adjustment of the shallow crust through strike-slip motions on a multitude of scattered small fault planes. Furthermore, the predominance of strike-slip faulting during seismic swarms occurs when the fluid overpressure induces horizontal propagation of vertical fractures with strike-slip motions, followed by horizontal fluid flow.

Key words: Yellowstone; seismicity; fractures; earthquakes; fault; stress;

1. Introduction

An accurate evaluation of present seismicity in terms of fault kinematics and temporal and spatial changes in the stress field is a core component of an assessment of the connection between seismic and magmatic processes, and thus useful for a better comprehension of seismic and volcanic hazards (Waite and Smith, 2004). In fact, earthquakes probe the state of stress in the upper crust, complementary to ground deformation with co-located origin. In this study, we focus on the Yellowstone caldera, located in the 1300-km-long Intermountain Seismic Belt (western United States, Figure 1; Smith and Arabasz, 1991), characterized by high volcanic and seismic activity, with an annual rate of 1500-2000 earthquakes per year (Farrell et al., 2009).

Much of the seismicity in Yellowstone occurs as seismic swarms, which are characterized by a large number of earthquakes clustered in space and time (Farrell, 2007; Massin et al., 2013). Many periods of intense seismic swarm activity have been accompanied by geodetically-measured deformation modeled as responses to inflation and deflation of magmatic sills (e.g., Wicks et al., 2006; Chang et al., 2007, 2010; Russo et al., 2017). These processes are clearly linked (Waite and Smith, 2002; Shelly et al., 2013). For example, a particularly large seismic swarm that occurred on the northwest caldera rim in 1985 (Figure 2) occurred in concomitance with caldera wide subsidence and was attributed to magmatic or hydrothermal fluid flow that originated from beneath the Mallard Lake resurgent dome and migrated out of the caldera, causing earthquakes once they reached the brittle crust (Waite and Smith, 2002). Another earthquake swarm in January 2010 occurred in the same area (Figure 2; Shelly et al., 2013) at the onset of a five-month period of subsidence of the inner caldera (Chang et al., 2010).

Episodes of surface deformation have also occurred at the northwest caldera margin near Norris Geyser Basin. One notable period began with uplift in the latter half of 2013, at rates of over 15 cm/yr, through March 2014. The M_w 4.8 earthquake on March 30, 2014 in the Norris Geyser Basin area, the largest since 1980, (Farrell et al., 2014; Stovall et al., 2014) coincided with a rapid reversal to subsidence at a very high rate (over 20 cm/yr). At other times, vertical motions within the caldera are opposite of those on the northwest margin and have been linked to variations of flux of magmatic fluids from the caldera to the Norris-Mammoth fault corridor (Wicks et al., 2006; Dzurisin et al., 2012). In fact, at Yellowstone and other similar volcanotectonic settings, recognizing possible precursors of threatening volcanic processes and understanding how magma transfer can trigger them are key scientific challenges (Acocella, 2006).

Analysis of earthquake source mechanisms at Yellowstone in prior studies has demonstrated a link between caldera deformation and Focal Mechanism Solutions (FMS) (e.g., Waite and Smith; 2004; White et al., 2009; and Russo et al., 2017). Here we expand the focal mechanism catalog from Russo et al. (2017), which analyzed data from 1988-2009, by including 10,201 additional relocated earthquakes occurring between 2010 and 2016. We selected the best located 2,080 earthquakes and computed 224 new well-constrained, double-couple FMS for detailed analysis.

The questions we address here are: *i)* Are there systematic patterns of deformation that can be identified by grouping earthquake source mechanisms in terms of space and time? *ii)* What is the influence of past sill intrusions on the most recent stress field? *iii)* Which process causes the concurrence of normal and strike-slip kinematics? *iv)* What are the relationships between fault kinematics, stress changes and magmatic processes? *v)* What magmatic processes (fluid properties, dimensions, and dynamics) might have been occurring?

2. Geological and structural settings

2.1 Geological overview

Even though no magmatic eruptions have occurred at the Yellowstone volcanic plateau since ~70 ka ago within or near the caldera, the area is still volcanically active, with high hydrothermal and seismic activity and periods of magmatic-fluid-triggered deformation well-documented by Global Navigation Satellite Systems (GNSS) and Interferometric Synthetic Aperture Radar (InSAR) data recorded over the past several decades (e.g., Wicks et al., 2006; Chang et al., 2007, 2010). The Yellowstone region is located in the northeastern part of the extending Basin and Range Province, 1600 km east of the western North American plate boundary (inset in Fig. 1A). According to measurements of fault plane striations and seismic data, the direction of tectonic extension is: *i)* E-W in southern Yellowstone; *ii)* NE-SW to the north and west of Yellowstone (Fig. 1B); and *iii)* locally N-S in the area of the 1959 M7.3 magnitude Hebgen Lake earthquake (Doser, 1985; Eddington et al., 1986; Zoback, 1992).

The presence of a deep-seated mantle plume defines the nature of Yellowstone as an intraplate hotspot and is at the origin of a high total heat flux up to 1800 mW/m^2 (Fournier et al., 1976). Furthermore, Yellowstone lies at the northeast end of the eastern Snake River Plain, a northeast-trending structural depression about 350 km long (Kirkham, 1931; Malde and Powers, 1962). The Yellowstone Plateau is a clear example of a compositionally bimodal rhyolite-basalt

igneous field; no intermediate composition is present (Christiansen, 2001). The geological features in the area are the result of its violent volcanic past, consisting of three catastrophic caldera-forming eruptions at 2.1, 1.3 and 0.63 Ma, which erupted 2500 km^3, 280 km^3 and 1000 km^3 of material, respectively (Christiansen, 2001). Three major sheets of ash-flow tuffs make up the stratigraphic column, separated by unconformities: from oldest to youngest, *i)* the Huckleberry Ridge tuff, which corresponds to the development of the first caldera (2.1 Ma), *ii)* the Mesa Falls tuff (composed by the Island Park Rhyolite and Mount Jackson Rhyolite), which represents the second caldera formation (1.3 Ma), and *iii)* the Lava Creek tuff and the Plateau Rhyolite, corresponding to the 0.63 Ma Yellowstone caldera (Fig. 1B; Christiansen, 2001). The most recent eruption formed the 45 x 70 km Yellowstone caldera that overlies a 5-15% partially molten magma reservoir (Farrell et al., 2014).

2.2 Fault geometry and kinematics

The Yellowstone Plateau and the eastern Snake River Plain are outlined by mountain ranges and parallel valleys delimited by normal faults typical of the Basin and Range Province. These features trend N-S in the south and in the east of the region, whereas they trend NW to NNW in the northern and western part. The normal faults have an average length of 735 meters. The main Quaternary faults, shown in Figure 1B (after Christiansen, 2001), strike mostly from N to NNW, as shown by the rose diagrams presented in Figure 3A, consistently with several NNW alignments of post-caldera volcanic vents.

Christiansen (2001) distinguished these faults between certain and concealed, based on the reliability of the location of the structures: the latter structures have a poorly defined trace in the field and are inferred on the basis of topography, whereas certain faults have been mapped by photogrammetry on a topographic basemap at a scale of 1:250,000 or more detailed (Machette, 2001). These are all mapped as normal faults, although a detailed reconstruction of their kinematics that could indicate strike-slip components is not available. A decrease in measured vertical offset has been observed when approaching the caldera, because of the coverage by volcanic rocks on the plateau, whereas at distance it is possible to observe cumulative displacements on faults over time in the order of 396 m (Christiansen, 2001; Love, 1961). Faults are characterized in most cases by linear trends in plan view, except in some areas as for example just outside the northeastern caldera rim, where they have an arcuate shape. This shape has been considered as influenced by movements of the Yellowstone magmatic body at depth in an area

that did not have a strongly developed preexisting system of tectonic faults (e.g. Eaton et al., 1975). Waldrop (1969) showed that these faults have had renewed rupture during late Quaternary times. The relation between fault length and azimuth is shown in the graph in Figure 3B. The maximum fault length reaches 10.4 km, whereas the majority of faults have lengths comprised between 0.1 and 2 km. Azimuth values do not show preferential intervals.

The 0.63 Ma Yellowstone caldera (third cycle) has an elliptical shape, elongated in an ENE-WSW direction, and is characterized by the presence of two resurgent domes: the eastern Sour Creek dome, which formed soon after the caldera, and the western Mallard Lake dome, which dates to about 0.16 Ma (Christiansen, 2001). Each dome has a ring-fracture zone, which delineates the margin of the post-caldera uplifted blocks, and a series of NW-striking faults with an average length of 754 meters that form a complex graben along the structural axis (Fig. 1B). These faults are related to uplift and doming of the resurgent blocks, not to their collapse (Carr and Quinlivan, 1968; Smith, 1968). The youngest movements along these faults were recognized by Pierce (1973) as post-dating the last main glaciation of the Rocky Mountains (late Pleistocene).

2.3 Deformation during 2010-2016

Leveling, GPS, and InSAR measurements have captured periods of uplift and subsidence throughout the volcanic plateau (Pelton and Smith, 1979; Dzurisin et al., 1994; Wicks et al., 1998, 2006; Chang et al., 2007). These episodes of deformation within and adjacent to the caldera have been attributed to combinations of two processes taking place beneath the caldera: pressurization and de-pressurization of an alternately self-sealed and leaking hydrothermal fluid reservoir that traps volatiles exsolved from a crystallizing rhyolitic magma reservoir, or transfer, formation and crystallization of rhyolitic or basaltic magma (Wicks et al., 2006).

Previous studies (e.g. Chang et al., 2010) have shown that the vertical components of deformation recorded at two stations, WLWY and NRWY (see Fig. 1B), are representative of the 0.63 Ma caldera and the Norris Geyser Basin, respectively. These stations show different phases of deformation during the temporal window of our analysis (Figure 4): the caldera experienced subsidence from January 2010 at rates of about 1.5 cm/yr until the M_w 4.8 earthquake in March 2014, which was part of the Norris seismic swarm. This earthquake occurred at the same time of a reversal in the deformation from subsidence to uplift at about 10 cm/yr (Figure 4; Chang et al., 2010). Uplift in the Norris Geyser Basin area began in the second half of 2013, reaching rates of over 15 cm/yr in the beginning of 2014. After the 2014 Norris earthquake, deformation near

Norris reversed to rapid subsidence at a rate exceeding 20 cm/yr (Farrell et al., 2014; Stovall et al., 2014). In 2016, the 0.63 Ma Yellowstone caldera was subsiding, whereas the Norris Geyser Basin area was uplifting (Farrell, 2013). According to previous studies (e.g. Shelly et al., 2013), the crustal transfer of fluids outward from the caldera and inward from the Norris area could be the underlying cause of the deformation reversals observed in the Yellowstone area.

3. Methods

3.1 Hypocenter relocation and earthquake selection

The University of Utah Seismograph Stations (UUSS) has recently improved the Yellowstone seismic network, which consists of up to 47 short-period vertical and three-component broadband seismic stations (Figure 5B). The UUSS records and documents earthquakes, locates hypocenters, and produces public information and data for scientific research. We relocated a total of 10,201 earthquakes from the UUSS catalog (Figure 5A) using a nonlinear relocation approach known as NonLinLoc (Lomax et al., 2000) and a three-dimensional velocity model computed with local earthquake tomography (Farrell et al., 2014). This relocation approach assures the high-quality location and uncertainty parameters for each earthquake. We selected a subset of earthquakes with the aim of identifying the best-quality earthquake locations for FMS computation and stress-field inversion according to Yang et al. (2012).

We imposed the following criteria: i) 10 or more first-motion observations; ii) the ratio of the nearest station distance to hypocentral depth must be lower than 1.50; iii) the azimuthal gap must not exceed 180°; iv) the euclidian distance between the maximum likelihood and the center of the uncertainty ellipsoid (being fitted over the location PDF) given by the nonlinear location procedure must not exceed 500 m (larger differences can result from an ill-conditioned location problem, Lomax et al., 2000); v) the Root Mean Square residual must be lower than 0.5 seconds and vi) the average of location uncertainties be less than 2 km.

About 20% of the relocated events met all six criteria, yielding 2167 earthquakes for FMS analysis (Figure 5B).

The histograms in Figure 6 show the depth distribution of the whole set of relocated hypocenters and of the subset of selected earthquakes. Although most of the earthquakes in the relocated catalog are shallower than 8 km, the majority of these shallow earthquakes did not meet the criteria imposed to achieve high-quality FMS. In particular, the requirement that a

station must be within 1.5 times the focal depth severely restricts areas in which shallow events are located to be close to seismic stations. In other words, it biases the data set toward deeper events. In fact, the vast majority of the selected earthquakes (79%) were between 8 km and 12 km depth (Fig. 6B).

3.2 Focal mechanism solutions and stress field

We determined 224 new double-couple FMS out of 2167 selected earthquakes from 2010-2016 by using the program HASH (Hardebeck and Shearer, 2002), which fits P-wave first motion polarity to the double-couple focal mechanisms. While fluid-driven earthquakes may produce non-double-couple events, allowing non-double-couple events increases the ambiguitiy and we are using only P-wave first motions. Two non-double couple FMS that were robustly constrained in Yellowstone were interpreted to have been triggered by pressurized hydrothermal fluids in the upper crustal magma system (Taira et al., 2010).

Four parameters were used to define the quality of resulting solutions (Table 1): average misfit, Root Mean Square of the fault plane uncertainty, station distribution ratio, and mechanism probability (Hardebeck and Shearer, 2002). The majority of our data (96%, 216 FMS) is characterized by D quality, whereas no solutions are characterized by quality A, 2 have quality B, and 6 quality C. Qualities E and F have been discarded, due to their likely inaccuracy.

Kilb and Hardebeck (2006) found that the single best discriminator of solution quality was the RMS fault plane uncertainty. The majority of the solutions are rather low quality D which have no specific classification based on this parameter, but we found that 58% have a value between 35^{O} and 45^{O}, consistent with quality C.

The lack of highest-quality solutions is due in part to the fact that the solution quality scheme was developed for California, where station density of the network is higher than in the Yellowstone volcanic field.

Earthquakes are passive markers of deviatoric stress and individually determined FMS have been used to estimate the best uniform stress field within limited space-time windows through different procedures (Angelier, 1984; Gephart and Forsyth, 1984; Michael, 1987; Rivera and Cisternas, 1990; Horiuchi et al., 1995; Robinson and McGinty, 2000; Abers and Gephart, 2001; Hardebeck and Shearer, 2003; Hardebeck, 2006). In our study, we use a new iterative stress

inversion method, known as STRESSINVERSE, that modifies Michael's method (Michael, 1987) and inverts jointly for stress and fault orientations (Vavrycuk, 2014).

4. Results

4.1 Spatial and temporal distribution of earthquakes

The 10,201 relocated earthquakes are distributed throughout the Yellowstone volcanic plateau and the areas of especially concentrated seismicity are shown with black rectangles in Fig. 5A. One E-W-trending cluster northwest of the 0.63 Ma Yellowstone caldera lies between Norris Geyser Basin and the 1959 Hebgen Lake earthquake epicenter. A second region of concentrated seismicity occupies the NW caldera, north of the Mallard Lake resurgent dome and includes the 2010 Madison Plateau swarm (Shelly et al., 2013). Elsewhere, smaller clusters of seismicity are found within and adjacent to the 0.63-Ma caldera, especially near the southern margin and within Yellowstone Lake.

Most of the seismic swarms that have occurred since seismic recording at Yellowstone began in 1973 are within the area of these two main clusters of concentrated seismicity (Figure 2; Waite and Smith, 2002; Farrell et al., 2010; Shelly et al., 2013). These swarms, common in volcanic settings and associated with changes in crustal deformation from uplift to subsidence, have been attributed to stress changes induced by the movement of magmatic fluids in the subsurface (Chang et al., 2010). In particular, 1352 earthquakes of our new database (65%) were part of the 2010 Madison Plateau seismic swarm that occurred over a one-month period near the northwest boundary of the caldera (Massin et al.,2013; Shelly et al., 2013). This swarm, like the 2008-2009 swarm beneath Yellowstone Lake (Farrell et al., 2010) and the 1985 swarm in the northwestern part of the caldera (Waite and Smith, 2002), was driven by the release of magmatic fluids from the crustal reservoir to the surrounding area along pre-existing NNW-striking rupture zones (Shelly et al., 2013). Our database also contains 80 selected earthquakes from another earthquake swarm that occurred near the Norris Geyser Basin between September 2013 and June 2014, associated with the M_w 4.8 earthquake (Farrell et al., 2014; Stovell et al., 2014). As mentioned before, the deformation in the Norris area reversed from uplift to rapid subsidence shortly after this earthquake (Figure 4).

4.2 Focal mechanisms and kinematics

Figure 7 shows the new set of 224 double-couple FMS computed for the time period 2010-2016. Of the 224 FMS, 154 FMS show a strike-slip faulting mechanism, 23 FMS are normal, 30 are

normal-oblique, and 3 have a reverse-faulting mechanism. The strike-slip events are mostly associated with the 2010 Madison Plateau seismic swarm; in fact, a total of 146 earthquakes of our database (out of 224) are part of that seismic swarm.

The presence of normal and normal-oblique kinematics is expected given that the location of the Yellowstone volcanic plateau is within the Basin and Range Province (Fig. 1A), a region of NE-SW tectonic extension characterized by many listric and planar normal faults with opposing dip that produce a "horst and graben" geometry (Christiansen, 2001). Past studies of FMS (e.g., Waite and Smith, 2002; Russo et al., 2017) have shown that the majority of FMS are consistent with this regional trend.

4.3 Calculation of the stress field and relation with surficial deformation

FMS have been divided into temporal, spatial, and depth windows with an iterative, trial-and-error approach, in order to identify variations of the stress field within the Yellowstone region (Figs. 8-9-10). The upwarping and downwarping episodes of surficial deformation documented by GPS data (Fig. 4), have been correlated with the focal mechanism inversions of the coeval seismicity, in order to delineate the stress field associated with the deformation episodes. The WLWY and NRWY GPS stations have been chosen from among the Yellowstone network according to previous studies (e.g. Chang et al., 2010) as the most representative of surficial deformation within the Yellowstone caldera and the Norris Geyser Basin, respectively.

Regarding the spatial windows of analysis, we calculated the stress field of the inner 0.63 Ma Yellowstone caldera and the Norris Geyser Basin separately. Furthermore, we divided our data into 2 km depth intervals in order to analyze the variations of the stress field from the upper to the lower crust. This depth interval is slightly less than the estimated uncertainty of the earthquake locations; the average of the longest uncertainty ellipse axis, usually close to vertical, is 2.6 km, whereas the average of the shortest is 0.95 km. We interpret only the depth windows containing at least 6 events.

Focal mechanism solutions have also been divided according to their kinematics prior to stress field calculation, in order to perform a detailed investigation on temporal and spatial variations of faulting and related orientation of principal stress axes.

Figure 8 shows the results of focal mechanism inversions and related stress field of the inner part of the 0.63 Ma Yellowstone caldera divided into kinematics, depth, and temporal windows, according to phases of surficial deformation recorded at WLWY GPS station between

2010 and 2016. Strike-slip kinematics, occurring between the surface and 10 km, appear to be shallower than normal and normal oblique, which both extend down to 14 km depth, and in particular all the normal oblique faults are deeper than 6 km. According to our results, the stress field associated with the 2010 Madison Plateau seismic swarm, being characterized by normal oblique and strike-slip kinematics, is characterized by a nearly horizontal greatest principal stress (σ_1) with a NW-SE direction in the case of strike-slip faulting and NNW-SSE in the case of normal oblique faulting. By extending the temporal window of analysis to the subsidence stage up to 2014, we observe that: i) regarding normal-oblique faults, the extension direction has a NNE-SSW direction between 8 km and 12 km depth; ii) in the case of strike-slip faulting, by looking at the least principal stress (σ_3) directions, we notice a slight rotation from a NE-SW orientation to NNE-SSW between the 6-8 km and 8-10 km depth windows . A single normal oblique FMS during the stasis between late 2014 and late 2015 hints at the presence of normal oblique faults at the shallow levels (2-4 km). The smaller number of selected earthquakes during uplift is due to a lower quality of raw seismic data, which has been then discarded.

In Figure 9, we present the results of focal mechanism inversions and related stress field of the outer part of the 0.63 Ma Yellowstone caldera, in the Norris Geyser Basin, divided into kinematics, depth, and temporal windows, according to phases of surficial deformation recorded at NRWY GPS station between 2010 and 2013, during a period of low-rate subsidence. The deformation pattern associated with this phase is very heterogeneous, being characterized by normal, normal-oblique, strike-slip, and subordinate reverse faults, all of them located at depths > 4 km. By taking into account strike-slip faults, which represent the predominant kinematics and are characterized by depth windows with at least 6 events between 6 km and 12 km, we observe a clear clockwise rotation of both the σ_3 and σ_1 directions, differently from the case of the inner part of the Yellowstone caldera (Figure 8), where only a slight rotation of σ_3 is observed.

Focal mechanisms inversion in the Norris Geyser Basin from 2013 on (Figure 10) has not been performed due to the fact that all depth windows contain less than 6 seismic events and thus are not considered reliable.

5. Discussion

Seismicity in the Yellowstone caldera occurs both by clusters and by more scattered events. Our FMS results indicate a complexity of fault slip with the predominance of strike-slip motions

during clustered seismic swarms, and subordinate normal motions; both kinematics take place with different relative percentages during diverse magmatic-tectonic processes. We thus describe in the following sections: i) the possible control of regional tectonics on preferential orientation of faults, and ii) a distinct interpretation of the different origins of fault slip during seismic swarms, sill emplacement and deflation phases.

5.1 Seismic clusters and slip planes

In map view, the epicenters of the 10,201 relocated earthquakes tend to focus in two main groups, shown with black rectangles (Fig. 5A): *i)* one located north of the Mallard Lake dome, which coincides with the 2010 Madison Plateau and 1985 seismic swarm locations (Fig. 2) (Massin et al., 2013; Shelly et al., 2013), and *ii)* another group more to the north, in the Norris Geyser Basin area, whose events occurred from September 2013 to June 2014. At higher detail, the group north of the Mallard Lake dome is composed of four N-S- to NNW-SSE-elongated clusters. In the western part of the Norris Geyser Basin area, there is a wide cluster with no clear elongation, whereas in the eastern part there is another N-S-elongated cluster. This orientation is similar to the NNW-SSE elongation of smaller clusters at the southern margin of the 0.63-Ma caldera and to the N-S elongation of the 2008-2009 Yellowstone Lake swarm (Fig. 2). The NNW-SSE to N-S range coincides with the dominant strike of the Quaternary normal faults present in the whole area (Figs. 1 and 3). This is also consistent with the FMS obtained in the present work that have slip planes that strike NW-SE to NNW-SSE, perpendicular to the regional σ_3 orientation (Zoback, 1992). The stress orientation based on our seismic analyses, typically horizontal NE-SW σ_3 especially during the uplift phases at the Yellowstone caldera, is also consistent with the regional σ_3 direction of the Basin and Range Province. We thus suggest that the orientation of dominant coseismic faulting may be influenced by regional tectonics, irrespective of magmatic or tectonic origin of fault slips.

The unclear orientation of the group of earthquakes in the western part of the Norris Geyser Basin area, might also depend upon the influence of a fracture network constituted by a larger range of planes striking WNW-ESE to N-S. This suggestion is consistent with the larger scattering of σ_3 directions in the Norris Geyser Basin area and with the complexity of the fault network and of temporal and spatial evolution of faulting during the 2017 Maple Creek earthquake swarm (Shelly and Hardebeck, 2019; Pang et al., 2019).

5.2 Relation between seismic swarms and strike-slip motions

Seismic swarms (Fig. 2) are common in the Yellowstone plateau volcanic history (Waite and Smith, 2002; Farrell et al., 2010; Shelly et al., 2013), as well as in volcanic settings in general, and are frequently attributed to the movement of magmatic fluids in the subsurface. Fluid propagation can be accompanied by enlargement of pre-existing fractures and/or the development of new fractures and small faults. At Yellowstone, the 1985 and 2010 seismic swarms occurred in concomitance with or at the beginning of a period of caldera subsidence, suggesting that fluid escape along the coseismic fractures may have originated a decrease of pressure beneath the caldera floor and the consequent downsagging.

To explain the concomitance of normal and strike-slip motions during the 2010 Madison Plateau seismic swarm revealed by our FMS, we adopt the model represented in Figure 11, which is based on the concept developed by Ágústsdóttir et al. (2016) and Ruch et al. (2016) for the 2014 Bárðarbunga-Holuhraun dyke intrusion, and on the strike-slip components measured along volcano-tectonic fractures in north Iceland by Bonali et al. (2019a,b). We note that also the 1985 swarm was characterized by the presence of strike-slip and oblique strike-slip FMS (Waite and Smith, 2002). This model suggests that overpressurized fluids can start to escape from the main magmatic body following a suitably-oriented vertical fracture. At the advancing fluid tip, a new fracture can develop at an oblique angle in response to stress concentration (Pollard and Holzhausen, 1979; Bonafede and Olivieri, 1995). If the fluid plane propagates upward, normal faults with converging dips may form (Fig. 11A), followed by upward fluid flow. If the vertical fluid plane propagates horizontally, left-lateral or right-lateral strike-slip faults might form at oblique angles (Fig. 11B), followed by horizontal fluid flow. These faults have left-lateral motions if oriented clockwise with respect to the strike of the main fluid plane, and right-lateral if rotated anticlockwise. After the faults are formed, the fluid may advance by intruding into one of the two faults, thus inducing opening of the fault plane.

5.3 Fault slip and sill development from 1988 to 2016

We contrast the new FMS catalog with the 1988-2009 data by Russo et al. (2017), where the same kind of analysis has been performed, to more fully interpret the association between faulting kinematics and deformation. In the 1988-2009 period analyzed by Russo et al. (2017), the majority of earthquakes (58%) are associated with a normal faulting mechanism, followed by 40%

associated with strike-slip faulting and subordinate reverse faulting. Normal faults occurred mostly (93%) between the near-surface and a depth of 10 km, thus indicating that brittle deformation has developed also at the shallowest level under extension. These authors found no relation between the orientation of fault planes revealed by FMS and the GPS-measured phases of surficial deformation. Nevertheless, they found that strike-slip faults were present along the northern front of the uplifting zone, which has been related to the inflation of a sill between 2004 and 2009 within the 0.63 Ma caldera (Chang et al., 2007, 2010). These faults were the result of a secondary, widespread adjustment of the shallow crust as block-faulting, showing that the rocks surrounding an inflating sill may accommodate deformation by transcurrent faulting. These results complement the classical model of extensional fracturing at the tip of an intruding horizontal magma sheet (Malthe- Sørenssen et al., 2004; Kavanagh et al., 2006). Normal motions instead, can be attributed to the extension that takes place in the extrados zone of an upwarping fold-like structure under the pressure of the inflating sill (Fig. 12).

The rarer occurrence of normal motions in the 2010-2016 period with respect to the previous time window, can be explained by the change in the surficial deformation shown by GPS data, which reveals a switch between uplift (pre-2010) and subsidence (2010-2016) (Figure 4). In 2010, in fact, the sill inflation ended causing a continuous contraction of the overburden. This contraction has been accommodated by structural adjustment in the form of strike-slip motions on a multitude of small fault planes, thus providing a further explanation on the occurrence of strike-slip kinematics apart from the model of seismic swarm development of Figure 11B. The distribution of deformation at several small faults is consistent again with the low magnitudes of the seismic events (Fig. 13B). Massin et al. (2013) assumed that multiplets could be defined as groups of earthquakes produced by re-activation of a self-similar seismic source, and showed that they preferentially occur during crustal subsidence episodes, and interpreted this as due to the preferential re-activation of pre-existing structures rather than the occurrence of neo-faulting. This is consistent with our data, where scattered strike-slip motions may be the effect of reactivation of already existing fractures under contraction.

5.4 Pervasive extensional stress and the missing eruption

During the sill inflation phases, which occurred in pre-2010 times (Chang et al., 2007, 2010; Wicks et al., 2006; Tizzani et al., 2015), the dominance of normal-faulting indicates the overburden was under a extensional state of stress (Russo et al., 2017). This implies that magma moved

horizontally (sill emplacement) even though the coeval stress state was characterized by horizontal σ_3 and a frequently horizontal intermediate principal stress (σ_2), which would seem to favor upward migration of fluids. Magma upwelling, giving rise to dykes and possibly eruptions, is in fact classically envisaged along vertical fractures coinciding with planes containing σ_2 and σ_1 and normal to σ_3 (Odé, 1957; Muller and Pollard, 1977).

Recently (Gonnermann and Taisne, 2015) proposed that the reason basaltic intrusions typically fail to reach the surface is due to the relatively small volumes of available melt. Tomography studies and petrologic modeling suggest that magma reservoirs are not continuous but rather composed of distributed pockets of melt.

At Yellowstone, only one explanation has been proposed to explain the lack of eruptions in recent times: Christiansen (2001) suggested that the rising of basaltic magmas is here inhibited because of the presence of the uppermost unconsolidated rhyolites that have higher viscosity and lower density with respect to the less viscous and denser basalts. Anyway, this explanation has been put forward before acknowledging that magma emplaces horizontally at Yellowstone and does not take into account the results of the present work indicating a very favourable stress state. We thus propose a more structural/mechanical explanation for this situation, based on the following series of observations: *i)* The hypocenter distribution shows that the brittle failure of rocks is scattered in all the examined rock volume in the pre-2010 period (Russo et al., 2017). In fact, the overall diffuse distribution of hypocenters testifies to a poorly defined pattern in most of the studied area, especially in a vertical section. This suggests that a main mechanical discontinuity from the depth of the magma chamber to the surface (through-going fracture) has not developed yet in most of the caldera floor. This is consistent with the low magnitudes of seismic events from 1988-2009, which indicate faulting with small offset (in the order of few cm) and slip planes (Fig. 13A). An exception is represented by the eastern part of the caldera, where the magma chamber is shallower (Farrell et al., 2014) and where more organized N-S alignments of hypocenters suggest a possible fracture zone from a depth of 6-8 km up to 2 km depth.

In fact, this region corresponds to the 2008-2009 Yellowstone Lake swarm, that was interpreted as resulting from shallow dyke emplacement (Farrell et al., 2010; Massin et al., 2013). Other possible old and deep fracture zones may have been sealed by the intense gas migration or may not be suitably-oriented with respect to stresses (Simakin and Ghassemi, 2010).

ii) Above the new sills there are strata of poorly permeable rocks that act as a trap (Dzurisin et al., 1994), possibly represented by older sills with a high mechanical strength. This can also create a local stress barrier to vertical dyke propagation, as suggested elsewhere (Gudmundsson, 2011; Geshi et al., 2012), leading to further sill emplacement (Tibaldi and Pasquarè, 2008).

iii) Sill emplacement induces arching of the overburden that, in turn, generates horizontal extension in the extrados as testified by the dominance of normal faulting during sill emplacement periods. Arching of the overburden generates also compression in the intrados (i.e. lower) zone, which lies immediately above the sill zone (Fig. 12). Finite element modelling showed that compression of the intrados and tension in the extrados might also be related to dyke intrusions along a caldera border (Saunders, 2004).

These three observations indicate that the overburden of Yellowstone includes a limited diaphragm of rocks where rock stiffness and stresses act as a barrier to magmatic intrusion, and where through-going fractures did not develop. Different forces are necessary for magma intrusion in intact host rocks (or poorly fractured rocks) versus intrusion in rocks affected by continuous long faults. Dyking can occur through a syn-intrusion fracture if magmatic pressure exceeds the lithostatic pressure, plus the horizontal compressive stress in the host rocks perpendicular to the dyke, plus the host rock tensile strength (Gudmundsson, 1995). With a horizontal σ_1 in the intrados of the poorly fractured arching overburden, we suggest that a very large magma overpressure is necessary to overcome the resistance forces and thus magma is favoured to migrate horizontally, similar to seismic results for the Yellowstone upper-crustal magma reservoir (Jiang et al., 2018). This explanation can be also applied to other unrest calderas in the world, such as Campi Flegrei where sill emplacement and horizontal σ_3 have also been recognized (Saccorotti et al., 2007), or at Toba caldera (Jaxybulatov et al., 2014) where multiple sill intrusions have been detected.

6. Conclusions

We relocated 10,201 earthquake hypocenters of the Yellowstone volcanic plateau, and calculated 224 new well-constrained, double-couple focal mechanism solutions and stress field for the period 2010-2016. These earthquakes were analyzed in terms of location, time, and kinematics according to the most recent phases of surficial deformation documented by GPS data, and were compared with the 1988-2009 seismicity in order to reveal systematic patterns of deformation and unravel their origin.

A strong predominance of strike-slip faulting solutions, and subordinate normal faulting, has been observed during the 2010 Madison Plateau seismic swarm. The σ_3 is horizontal and trends NE-SW to ENE-WSW, an orientation that is consistent with the regional extension. Considering the hypocenter locations more generally, the elongation of earthquake clusters is commonly N-S to NNW-SSE, coinciding with the strike of the Quaternary normal faults that crop out in the area. These data suggest that the orientation of brittle planes of deformation in the Yellowstone caldera and in the Norris Geyser Basin area is mostly controlled by regional tectonics.

We propose two different magmatic processes to explain the large number of strike-slip earthquakes and their concurrence with normal kinematics. During the 2010-2016 time window, subsidence of the Yellowstone caldera did occur as a consequence of the ending of magmatic sill inflation. This was accompanied by contraction of the overburden with structural adjustments of this shallow section of the crust mainly by strike-slip motions on a multitude of small fault planes, given also the low magnitude of seismic events. On the other hand, during 1988-2009, sill intrusions were accompanied by uplift and dominant normal faulting in the overburden, and subordinate strike-slip faulting around the uplifting area. In this case, extensional faulting may be related to arching of the extrados of the overburden, whereas compression in the intrados and stress barriers due to stiff rock layers might inhibit magma upwelling. These considerations shed lights on the influence of past sill intrusions on the deformation pattern.

For the 2010 Madison Plateau seismic swarm, we propose different mechanism for strike-slip faulting, related to the propagation of fluids towards the outer Yellowstone caldera. When the fluid overpressure induces horizontal propagation of vertical fractures, strike-slip motions may develop, followed by horizontal fluid flow. If there is upward fracture propagation, this may produce normal faulting followed by upward magma flow.

Acknowledgments

We acknowledge three anonymous reviewers for the useful suggestions on a previous version of the manuscript. This work is a contribution to the International Lithosphere Program - Task Force II. Part of the work has been done in the framework of a MIUR PhD funding to ER.

Bibliography

Abers, G.A., Gephart, J.W., 2001. Direct inversion of earthquake first motions for both the stress tensor and focal mechanisms and application to southern California. J. Geophys. Res. 106.

Acocella, V., 2006. Regional and local tectonics at Erta Ale caldera, Afar (Ethiopia). Journal of Structural Geology, 28(10), 1808-1820.

Ágústsdóttir, T., Woods, J., Greenfield, T., Green, R. G., White, R. S., Winder, T., Brandsdóttir, B., Steinthórsson S., Soosalu, H., 2016. Strike-slip faulting during the 2014 Bárðarbunga-Holuhraun dike intrusion, central Iceland. Geophysical Research Letters, DOI: 10.1002/2015GL067423.

Angelier, J., 1984. Tectonic analysis of fault slip data sets. J. Geophys. Res. 89 (B7), 5835–5848.

Bonafede, M., Olivieri, M., 1995. Displacement and gravity anomaly produced by a shallow vertical dyke in a cohesionless medium. Geophysical Journal International 123, 639-652.

Bonali, F. L., Tibaldi, A., Mariotto, F. P., Saviano, D., Meloni, A., Sajovitz, P., 2019a. Geometry, oblique kinematics and extensional strain variation along a diverging plate boundary: The example of the northern Theistareykir Fissure Swarm, NE Iceland. Tectonophysics, 756, 57-72.

Bonali, F. L., Tibaldi, A., Marchese, F., Fallati, L., Russo, E., Corselli, C. and Savini, A., 2019b. UAV-based surveying in volcano-tectonics: An example from the Iceland rift. Journal of Structural Geology, 121, 46-64.

Carr, W. J., Quinlivan, W. D., 1968. Structure of Timber Mountain resurgent dome, Nevada Test Site, in Eckel, E. B., ed., Nevada Test Site: Geological Society of America Memoir 110, p. 99-108.

Chang, W. L., Smith, R. B., Wicks, C. Farrell, J. M., Puskas, C. M., 2007. Accelerated uplift and magmatic intrusion of the Yellowstone caldera, 2004 to 2006, *Science*, 318, 952.

Chang, W. L., Smith, R. B., Farrell, J., Puskas, C.M., 2010. An extraordinary episode of Yellowstone caldera uplift, 2004-2010, from GPS and InSAR observations, *Geophysical Research Letters*, 37 (23).

Chang, W.L., R. B. Smith, Puskas, C.M., 2013. Effects of lithospheric viscoelastic relaxation on the contemporary deformation following the 1959 Mw 7.3 Hebgen Lake, Montana, earthquake and other areas of the intermountain seismic belt, Geochem. Geophys. Geosyst., 14, 1–17, doi:10.1029/2012GC004424.

Christiansen, R. L., 2001. The Quaternary and Pliocene Yellowstone plateau volcanic field of Wyoming, Idaho and Montana, *U.S. Geol. Surv. Profess. Pap.*, 729-G, 145.

D'Auria, L., Massa, B., Cristiano, E., Del Gaudio, C., Giudicepietro, F., Ricciardi, G., Ricco, C., 2015. Retrieving the stress field within the Campi Flegrei caldera (Southern Italy) through an integrated geodetical and seismological approach. Pure and Applied Geophysics, 172(11), 3247-3263.

Doser, D. I., 1985. Source parameters and faulting processes of the 1959 Hebgen Lake, Montana, earthquake sequence. Journal of Geophysical Research: Solid Earth, 90(B6), pp.4537-4555.

Dzurisin, D., K. M. Yamashita, J. W. Kleinman, 1994. Mechanisms of crustal uplift and subsidence at the Yellowstone caldera, Wyoming, *Bull. Volcanol.*, 56, 261-270.

Dzurisin, D., Wicks, C. W., Poland, M. P., 2012. History of surface displacements at the Yellowstone Caldera, Wyoming, from leveling surveys and InSAR observations, 1923-2008 (No. 1788). US Geological Survey.

Eaton, G. P., Christiansen, R. L., Iyer, H. M., Pitt, A. M., Mabey, D. R., Blank, J. R., Jr., Zietz, I., Gettings, M. E., 1975. Magma beneath Yellowstone National Park: Science, v. 188, p. 787-796.

Eddington, P. K., Smith, R. B., Renggli, C., 1986. A study of tectonic activity in the Basin-Range Province and on the San Andreas Fault. No. 1: Kinematics of Basin-Range intraplate extension.

Farrell, J. M., 2007. Space-time seismicity and development of a geographical information system database with interactive graphics for the Yellowstone region (Doctoral dissertation, Department of Geology and Geophysics, University of Utah).

Farrell, J., Husen, S., Smith, R. B., 2009. Earthquake swarm and b-value characterization of the Yellowstone volcano-tectonic system. Journal of Volcanology and Geothermal Research, 188(1-3), 260-276.

Farrell, J., Smith, R.B., Taira, T.a., Chang,W. L., Puskas, C.M., 2010. Dynamics and rapid migration of the energetic 2008–2009 Yellowstone Lake earthquake swarm. Geophys. Res. Lett. 37 (19).

Farrell, J., Smith, R. B., Husen, S., Diehl, T., 2014. Tomography from 26 years of seismicity revealing that the spatial extent of the Yellowstone crustal magma reservoir extends well beyond the Yellowstone caldera. Geophysical Research Letters, 41(9), 3068-3073.

Farrell, J., Shelly, D. R., Smith, R. B., Puskas, C. M., Chang, W. L., 2014. The Mw4. 8 Norris Geyser Basin Earthquake of 30 March, 2014 and its Relationship to Crustal Deformation and Seismic Activity of the Yellowstone Volcanic System. In AGU Fall Meeting Abstracts.

Fournier, R. O., D. E. White, A. H. Truesdell, 1976. Convective heat flow in Yellowstone National Park, in Second United Nations Symposium on Development and Use of Geothermal Resources, U.S. Govt. Print. Off., Washington D.C., 731-739.

Gephart, J.W., Forsyth, D.W., 1984. An improved method for determining the regional stress tensor using earthquake focal mechanism data: application to the San Fernando earthquake sequence. J. Geophys. Res. 89 (B11), 9305–9320.

Geshi, N., Kusumoto, S., Gudmundsson, A., 2012. Effects of mechanical layering of host rocks on dike growth and arrest. Journal of Volcanology and Geothermal Research, 223, 74-82.

Gonnermann, H., & Taisne, B. (2015). Magma transport in dikes. In The Encyclopedia of Volcanoes (pp. 215-224). Academic Press.

Gudmundsson, A., 1995. The geometry and growth of dykes. In: Baer, G., Heimann, A. (Eds.), Physics and Chemistry of Dykes. Balkema, Rotterdam, 23–34.

Gudmundsson, A., 2011. Deflection of dykes into sills at discontinuities and magma-chamber formation. Tectonophysics, 500(1), 50-64.

Hardebeck, J.L., 2006. Homogeneity of small-scale earthquake faulting, stress, and fault strength. Bull. Seismol. Soc. Am. 96 (5), 1675–1688.

Hardebeck, J. L., P. M. Shearer, 2002. A new method for determining first-motion focal mechanisms, Bull. Seismol. Soc. Am., 92, 2264-2276.

Hardebeck, J.L., Shearer, P.M., 2003. Using S/P amplitude ratios to constrain the focal mechanisms of small earthquakes. Bull. Seismol. Soc. Am. 93 (6), 2434–2444.

Horiuchi, S., Rocco, G., Hasegawa, A., 1995. Discrimination of fault planes from auxiliary planes based on simultaneous determination of stress tensor and a large number of fault plane solutions. J. Geophys. Res. Solid Earth 100 (B5), 8327–8338.

Jaxybulatov, K., Shapiro, N. M., Koulakov, I., Mordret, A., Landès, M., Sens-Schönfelder, C., 2014. A large magmatic sill complex beneath the Toba caldera. Science, 346(6209), 617-619.

Jiang, C., B. Schmandt, J. Farrell, F.C. Lin, and K.M. Ward (2018), Seismically anisotropic magma reservoirs underlying silicic calderas, Geology, 46(8), 727-730, doi:10.1130/G45104.1.

Kavanagh, J. L., Menand, T., Sparks, R. S. J., 2006. An experimental investigation of sill formation and propagation in layered elastic media. Earth and Planetary Science Letters, 245, 799–813.

Kilb, D., & Hardebeck, J. L. (2006). Fault Parameter Constraints Using Relocated Earthquakes: A Validation of First-Motion Focal-Mechanism Data. BULLETIN OF THE SEISMOLOGICAL SOCIETY OF AMERICA, 96(3), 1140-1158.

Kirkham, V. R., 1931. Snake River downwarp. The Journal of Geology, 39(5), 456-482.

Lomax, A., Virieux, J., Volant, P., Thierry-Berge, C., 2000. Probabilistic earthquake location in 3D and layered models: introduction of a Metropolis-Gibbs method and comparison with linear locations. In: Thurber, C.H., Rabinowitz, N. (Eds.), Advances in Seismic Event Location. Kluwer Academic Publishers, Dordrecht/Boston/London, pp. 101–134.

Love, J. D., 1961. Reconnaissance study of Quaternary faults in and south of Yellowstone National Park, Wyoming. Geological Society of America Bulletin, 72(12), 1749-1764.

Lowenstern, J. B., Smith, R. B., Hill, D. P., 2006. Monitoring super-volcanoes: geophysical and geochemical signals at Yellowstone and other large caldera systems. Philosophical Transactions of the Royal Society A: Mathematical, Physical and Engineering Sciences, 364(1845), 2055-2072.

Machette, M. N., 2001. Map and data for Quaternary faults and folds in Wyoming (p. 153). US Geological Survey.

Malde, H. E., Powers, H. A., 1962. Upper Cenozoic stratigraphy of western Snake River Plain, Idaho. Geological Society of America Bulletin, 73(10), 1197-1220.

Malthe-Sørenssen, A., Planke, S., Svensen, H., Jamtveit, B., 2004. Formation of saucer-shaped sills. In: Breitkreuz, C. & Petford, N. (eds) Physical Sill Morphology and Emplacement Mechanisms Geology of High-Level Magmatic Systems. Geological Society, London, Special Publications, 234, 215–227.

Massin, F., Farrell, J., Smith, R. B., 2013. Repeating earthquakes in the Yellowstone volcanic field: Implications for rupture dynamics, ground deformation, and migration in earthquake swarms. Journal of Volcanology and Geothermal Research, 257, 159-173.

Michael, A.J., 1987. Use of focal mechanisms to determine stress: a control study. J. Geophys. Res. 92 (B1), 357–368.

Muller, O. H., D. D. Pollard, 1977. The stress state near Spanish Peaks, Colorado determined from a dike pattern, Pure Appl. Geophys., 115, 69–86.

Nagorsen-Rinke, S., Lee, J., Calvert, A., 2013. Pliocene sinistral slip across the Adobe Hills, eastern California–western Nevada: Kinematics of fault slip transfer across the Mina deflection. Geosphere, 9(1), 37-53.

Odé, H., 1957. Mechanical analysis of the dike pattern of the Spanish Peaks area, Colorado, Geol. Soc. Am. Bull., 68, 567–576.

Pang, G., Koper, K. D., Hale, J. M., Burlacu, R., Farrell, J., & Smith, R. B. (2019). The 2017–2018 Maple Creek Earthquake Sequence in Yellowstone National Park, USA. Geophysical Research Letters, 46(9), 4653-4663.

Pelton, J. R., Smith, R. B., 1979. Recent crustal uplift in Yellowstone National Park. Science, 206(4423), 1179-1182.

Pierce, K. L., 1973. Surficial geologic map of the Mammoth quadrangle and part of the Gardiner quadrangle, Yellowstone National Park, Wyoming and Montana: U.S. Geological Survey Miscellaneous Geologic Investigations Map I-64l, scale 1:62,500.

Pollard, D. D., Holzhausen, G., 1979. On the mechanical interaction between a fluid-tilled fracture and the Earth's surface. Tectonophysics, 53, 27-57.

Puskas, C. M., Smith, R. B., 2009. Intraplate deformation and microplate tectonics of the Yellowstone hot spot and surrounding western US interior. Journal of Geophysical Research: Solid Earth, 114(B4).

Rivera, L., Cisternas, A., 1990. Stress tensor and fault plane solutions for a population of earthquakes. Bull. Seismol. Soc. Am. 80 (3), 600–614.

Robinson, R., McGinty, P.J., 2000. The enigma of the Arthur's Pass, New Zealand, earthquake: 2. The aftershock distribution and its relation to regional and induced stress fields. J. Geophys. Res. 105 (B7), 16139–16150.

Ruch, J., Wang, T., Xu, W., Hensch, M., Jónsson, S., 2016. Oblique rift opening revealed by reoccurring magma injection in central Iceland. Nat. Commun. 7, 12352.

Russo, E., Waite, G. P., Tibaldi, A., 2017. Evaluation of the evolving stress field of the Yellowstone volcanic plateau, 1988 to 2010, from earthquake first-motion inversions. Tectonophysics, 700, 80-91.

Saccorotti, G., Petrosino, S., Bianco, F., Castellano, M., Galluzzo, D., La Rocca, M., Cusano, P., 2007. Seismicity associated with the 2004–2006 renewed ground uplift at Campi Flegrei Caldera, Italy. Physics of the Earth and Planetary Interiors, 165(1), 14-24.

Saunders, S. J., 2004. The possible contribution of circumferential fault intrusion to caldera resurgence. Bulletin of Volcanology, 67(1), 57-71.

Shelly, D. R., Hill, D. P., Massin, F., Farrell, J., Smith, R. B., Taira, T. A., 2013. A fluid-driven earthquake swarm on the margin of the Yellowstone caldera. Journal of Geophysical Research: Solid Earth, 118(9), 4872-4886.

Shelly, D. R., Hardebeck, J. L., 2019. Illuminating Faulting Complexity of the 2017 Yellowstone Maple Creek Earthquake Swarm. Geophysical Research Letters, 46(5), 2544–2552.

Simakin, A. G., Ghassemi, A., 2010. The role of magma chamber-fault interaction in caldera forming eruptions. Bulletin of Volcanology, 72(1), 85.

Smith, R. B., W.J. Arabasz, 1991. Seismicity of the Intermountain Seismic Belt, in *Neotectonics of North America*, edited by D.B. Slemmons, E.R. Engdahl, M.D. Zoback, and D.D. Blackwell, *Geological Society of America*, Boulder, Colorado.

Smith, R. L., 1968. Resurgent cauldrons. Mem. Geol. Soc. Amer., 116, 613-662.

Stovall, W. K., Cervelli, P. F., Shelly, D. R., 2014. Investigating Rapid Uplift and Subsidence Near Norris, Yellowstone, During 2013-2014. In AGU Fall Meeting Abstracts.

Taira, T., Smith, R. B., & Chang, W. L. (2010). Seismic evidence for dilatational source deformations accompanying the 2004–2008 Yellowstone accelerated uplift episode. Journal of Geophysical Research: Solid Earth, 115(B2).

Tibaldi, A., Pasquarè Mariotto, F. A., 2008. A new mode of inner volcano growth: the “flower intrusive structure”. Earth and Planetary Science Letters, 271(1), 202-208.

Tizzani, P., Battaglia, M., Castaldo, R., Pepe, A., Zeni, G., Lanari, R., 2015. Magma and fluid migration at Yellowstone Caldera in the last three decades inferred from InSAR, leveling, and gravity measurements. Journal of Geophysical Research: Solid Earth, 120(4), 2627-2647.

Vavryčuk, V., 2014. Iterative joint inversion for stress and fault orientations from focal mechanisms. Geophysical Journal International, 199(1), 69-77.

Waldrop, H. A., 1969. Late Quaternary faulting near Mirror Lake Yellowstone National Park, in Abstracts for 1968: Geological Society of America Special Paper 121, p. 643-644.

Waite, G. P., Smith, R. B., 2002. Seismic evidence for fluid migration accompanying subsidence of the Yellowstone caldera. Journal of Geophysical Research: Solid Earth, 107(B9).

Waite, G. P., Smith, R. B., 2004. Seismotectonics and stress field of the Yellowstone volcanic plateau from earthquake first-motions and other indicators. Journal of Geophysical Research: Solid Earth, 109(B2).

White, B. J. P., Smith, R. B., Husen, S., Farrell, J. M., & Wong, I. (2009). Seismicity and earthquake hazard analysis of the Teton–Yellowstone region, Wyoming. Journal of Volcanology and Geothermal Research, 188(1-3), 277-296.

Wicks Jr., C., W. Thatcher, D. Dzurisin, 1998. Migration of fluids beneath Yellowstone caldera inferred from Satellite radar interferometry, *Science*, 282, 458-462.

Wicks, C., Thatcher, W., Dzurisin, D., 2006. Uplift, thermal unrest and magma intrusion at Yellowstone Caldera, *Nature*, 440, 72-75.

Yang, W., Hauksson, E., Shearer, P. M., 2012. Computing a large refined catalog of focal mechanisms for southern California (1981–2010): Temporal stability of the style of faulting. Bulletin of the Seismological Society of America, 102(3), 1179-1194.

Zoback, M.L., 1992. First and second-order patterns of stress in the lithosphere: The World Stress Map Project, *J. Geophys. Res.*, 97(B8), 11,703-11,728.

Declaration of interests

☒ The authors declare that they have no known competing financial interests or personal relationships that could have appeared to influence the work reported in this paper.

☐The authors declare the following financial interests/personal relationships which may be considered as potential competing interests:

CreditAuthorStatement

Russo Elena: Conceptualization; Investigation; Writing - Original Draft
Tibaldi Alessandro: Conceptualization; Writing - Original Draft
Waite Greg: Methodology; Conceptualization; Resources
Bonali Fabio Luca: Methodology; Writing- Reviewing and Editing
Massin Fred: Resources; Writing- Reviewing and Editing
Farrell Jamie: Resources; Writing- Reviewing and Editing

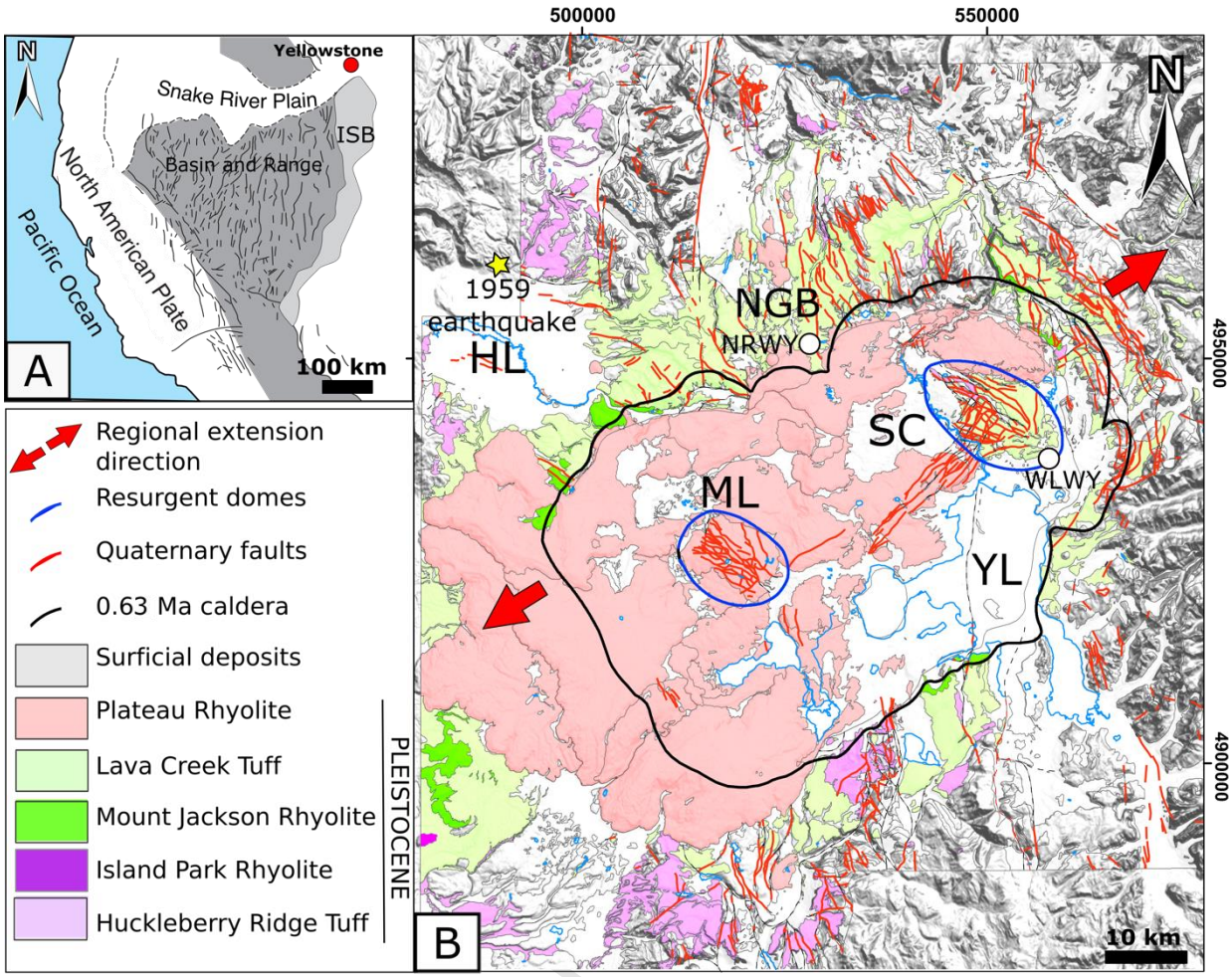

Figure 1: *(A) Inset showing location of Yellowstone volcanic plateau and main faults of Basin and Range Province (modified after Nagorsen-Rinke et al., 2013). ISB = Intermountain Seismic Belt. (B) Geological map of Yellowstone volcanic plateau modified after Christiansen (2001). ML = Mallard Lake resurgent dome; SC = Sour Creek resurgent dome; YL = Yellowstone Lake; HL = Hebgen Lake; NGB = Norris Geyser Basin. The 0.63 Ma caldera is shown as a black line, resurgent domes are represented as blue lines. Fault data, represented in red, after Christiansen (2001). Dashed lines indicate concealed faults. Red arrows represent the* σ_3 *direction (Puskas and Smith, 2009). Location of NRWY and WLWY GPS stations is shown as white circles. Shaded view of the Digital Elevation Model (DEM) provided by the USGS National Elevation Dataset. Coordinate system: WGS84/UTM zone 12N. Coordinates are expressed in meters. The WLWY and NRWY GPS stations have been chosen among the Yellowstone network according to previous studies (e.g. Chang et al., 2010) as the most representative of surficial deformations within the Yellowstone caldera and the Norris Geyser Basin, respectively.*

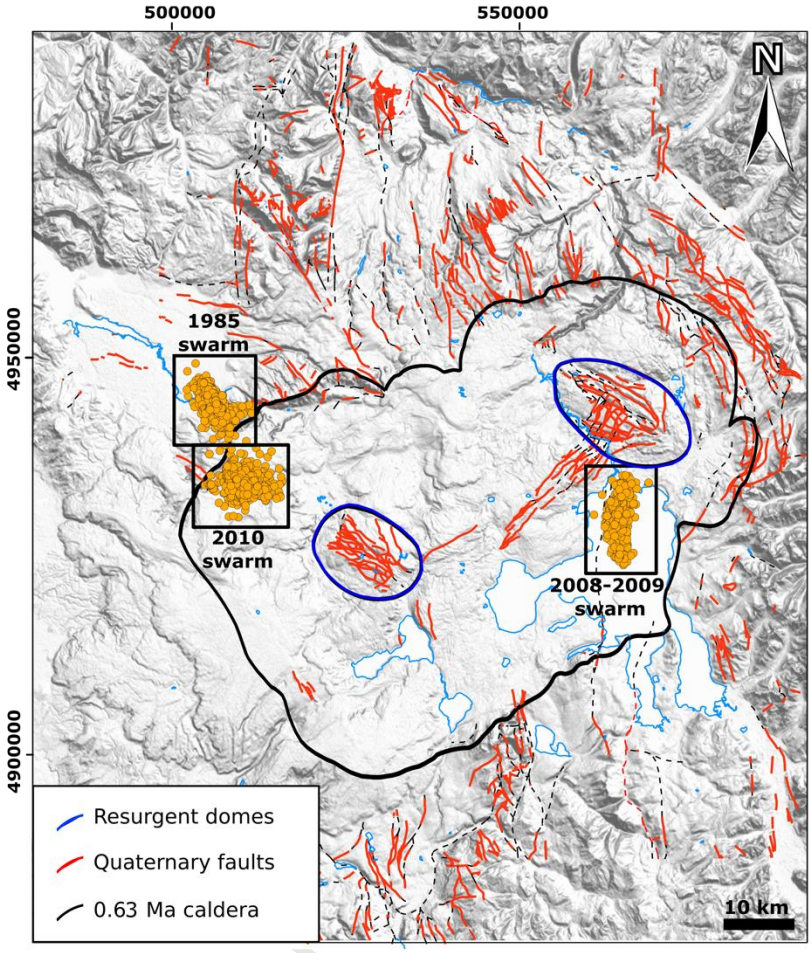

Figure 2: *Seismic swarms in the Yellowstone volcanic plateau. The black line is the 0.63 Ma Yellowstone caldera boundary, blue lines are the resurgent domes. Fault data, represented in red, after Christiansen (2001). Dashed lines indicate concealed faults. Shaded view of the Digital Elevation Model (DEM) provided by the USGS National Elevation Dataset. Coordinate system: WGS84/UTM zone 12N. Coordinates are expressed in meters. Earthquake catalogue is from USGS Earthquake Hazards program.*

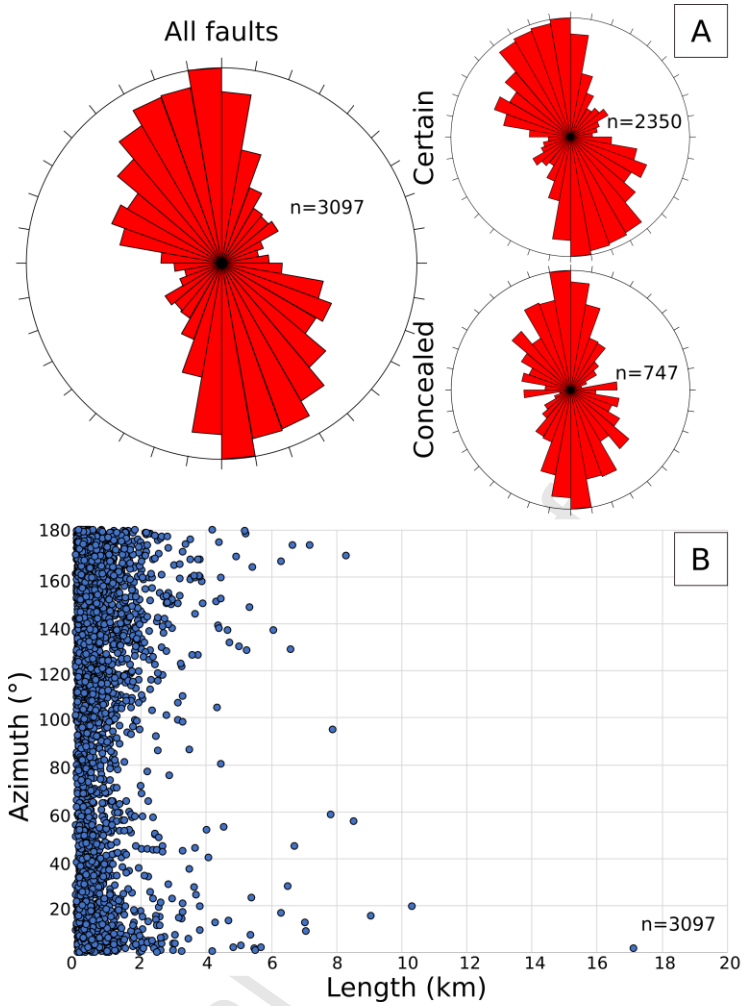

***Figure 3**: (A) Rose diagrams showing strike of Quaternary faults (after Christiansen, 2001), divided between 'certain' and 'concealed'. (B) Plot of the relation between length and azimuth of all faults (certain and concealed).*

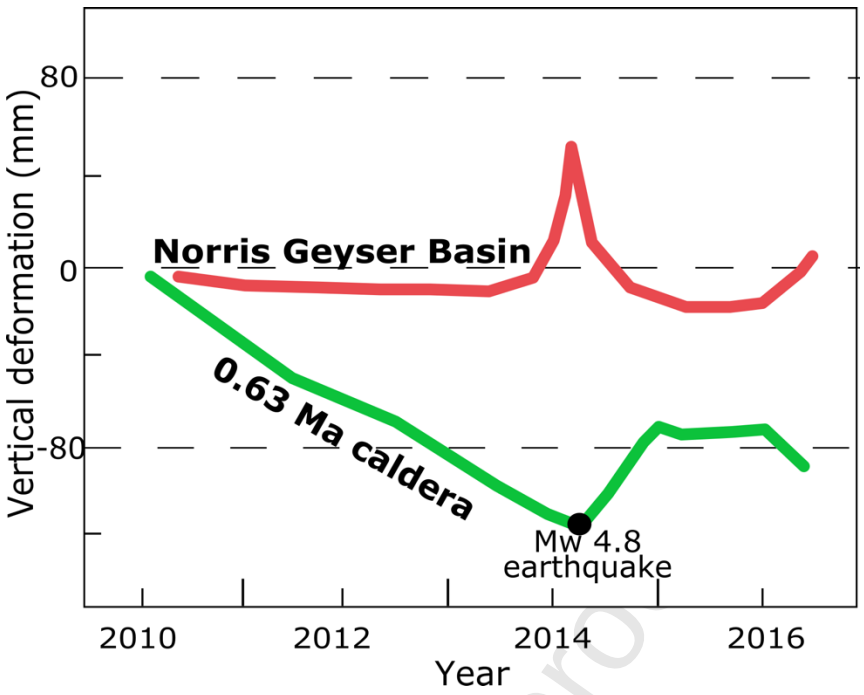

***Figure 4**: Vertical component of deformation documented by GPS stations WLWY and NRWY of the Yellowstone-Contin network between 2010 and 2016, representing intra-caldera and outer caldera (Norris Geyser Basin) deformation.*

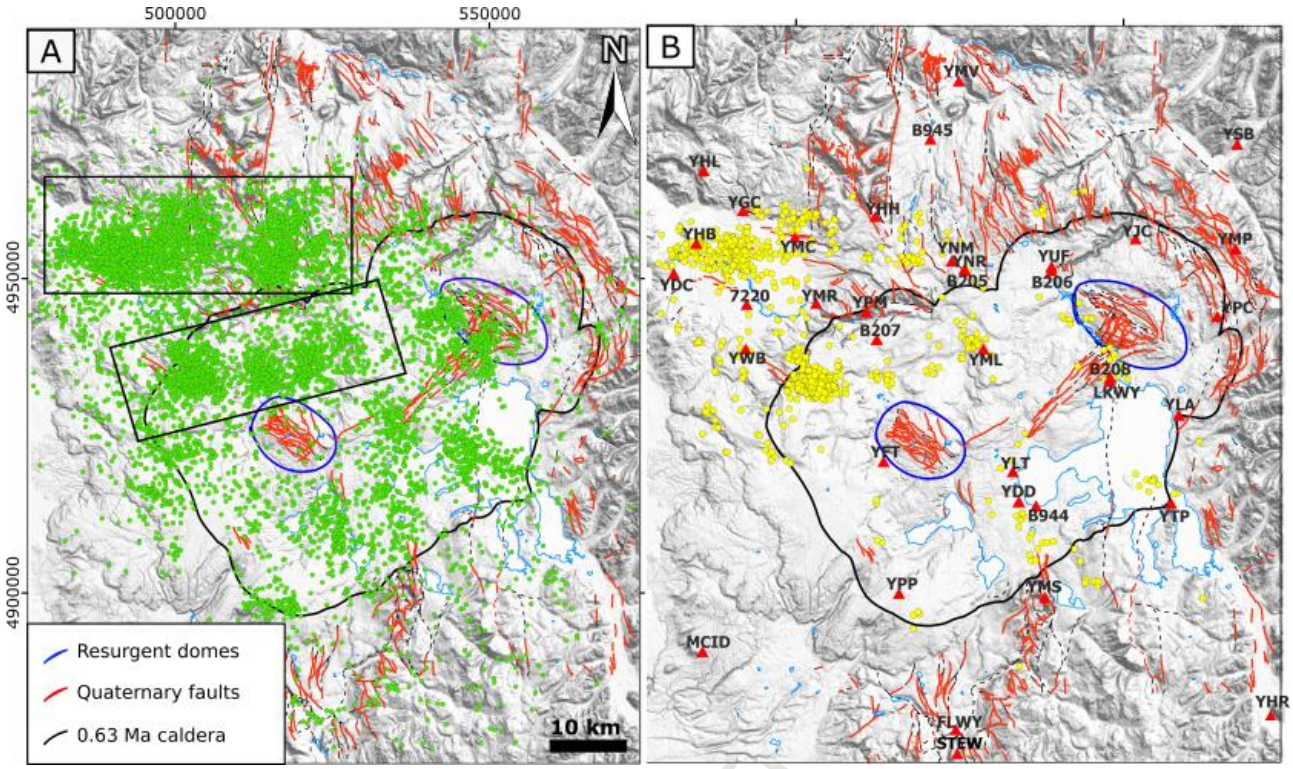

Figure 5: *(A) Total of 10,201 relocated earthquakes from 2010 to 2016 and (B) of the 2167 selected earthquakes. Seismic stations network is shown as red triangles. Fault data, represented in red, after Christiansen (2001). The 0.63-Ma-old Yellowstone caldera rim is outlined in black, the resurgent domes in blue. Black rectangles indicate main clusters of seismic activity. Dashed lines indicate concealed faults. Shaded view of the Digital Elevation Model (DEM) provided by the USGS National Elevation Dataset. Coordinate system: WGS84/ UTM zone 12N.*

Figure 6: *Depth distribution of the whole set of hypocenters (total of 10,201) (A) and of the subset of selected earthquakes (2167 earthquakes) (B).*

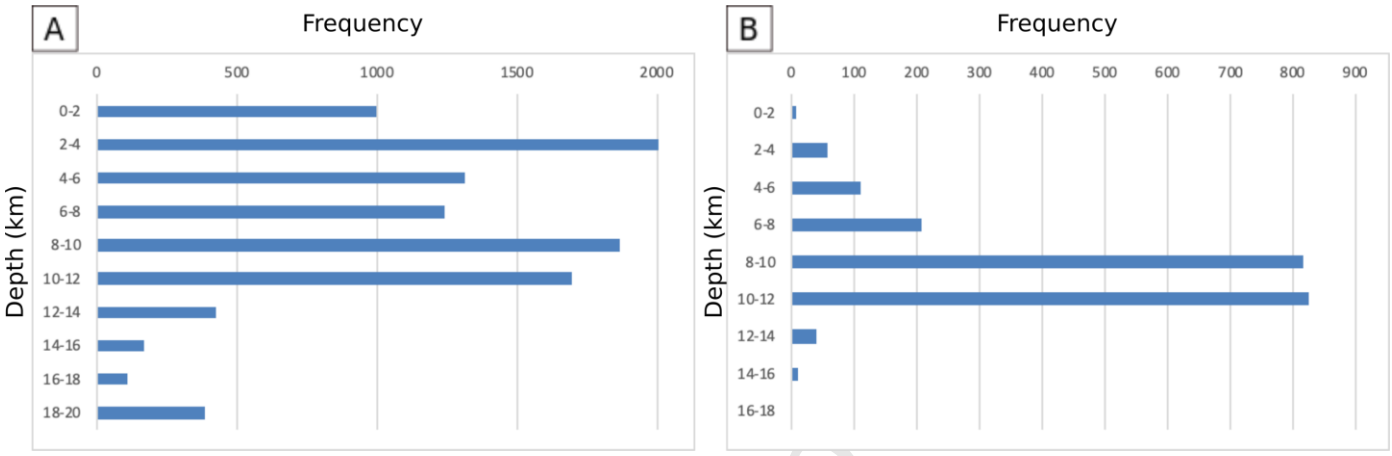

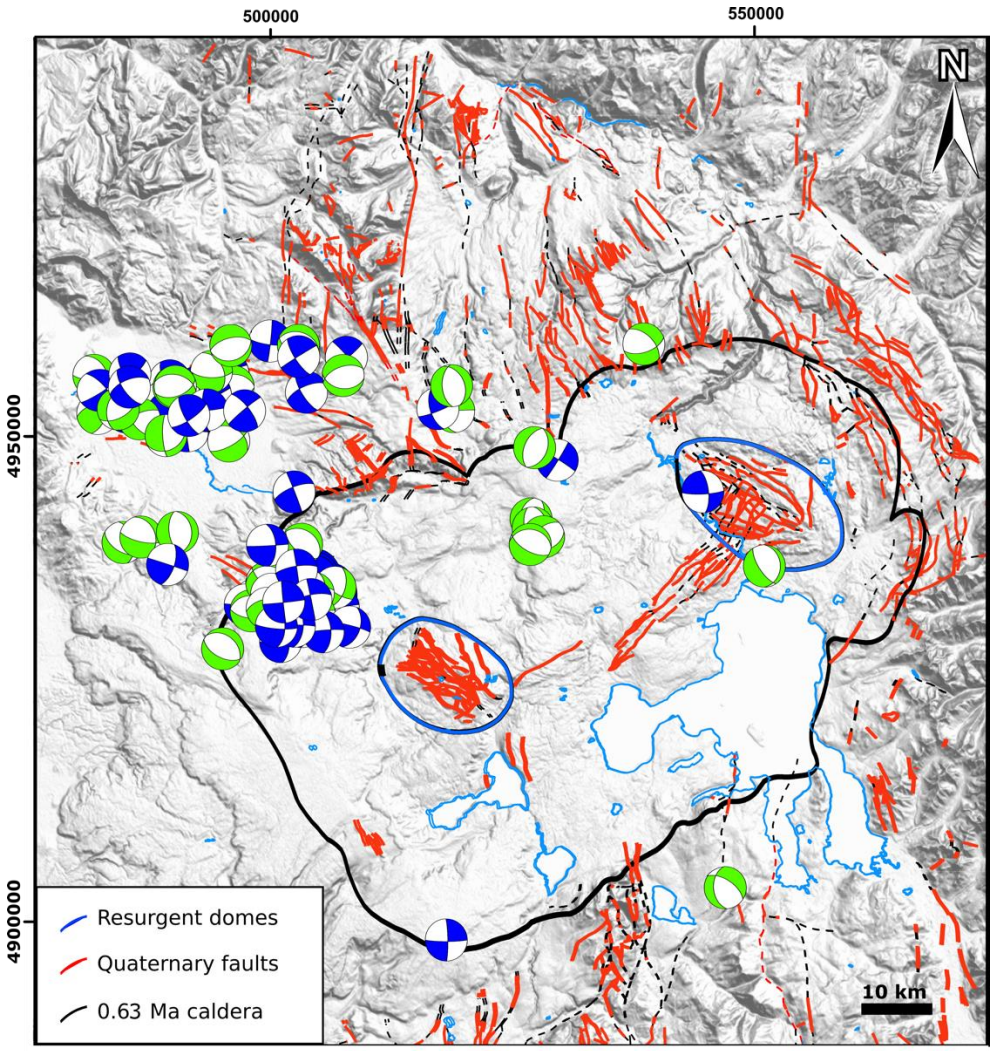

***Figure 7**: Complete set of 224 new double-couple focal mechanism solutions computed for the time period 2010-2016. Earthquakes are divided by kinematics: blue beach balls represent strike-slip faulting, green beach balls represent normal faulting. The black line is the 0.63 Ma Yellowstone caldera boundary, blue lines are the resurgent domes. Shaded view of the Digital Elevation Model (DEM) provided by the USGS National Elevation Dataset. Fault data, represented in red, after Christiansen (2001). Dashed lines indicate concealed faults. Coordinate system: WGS84/UTM zone 12N.*

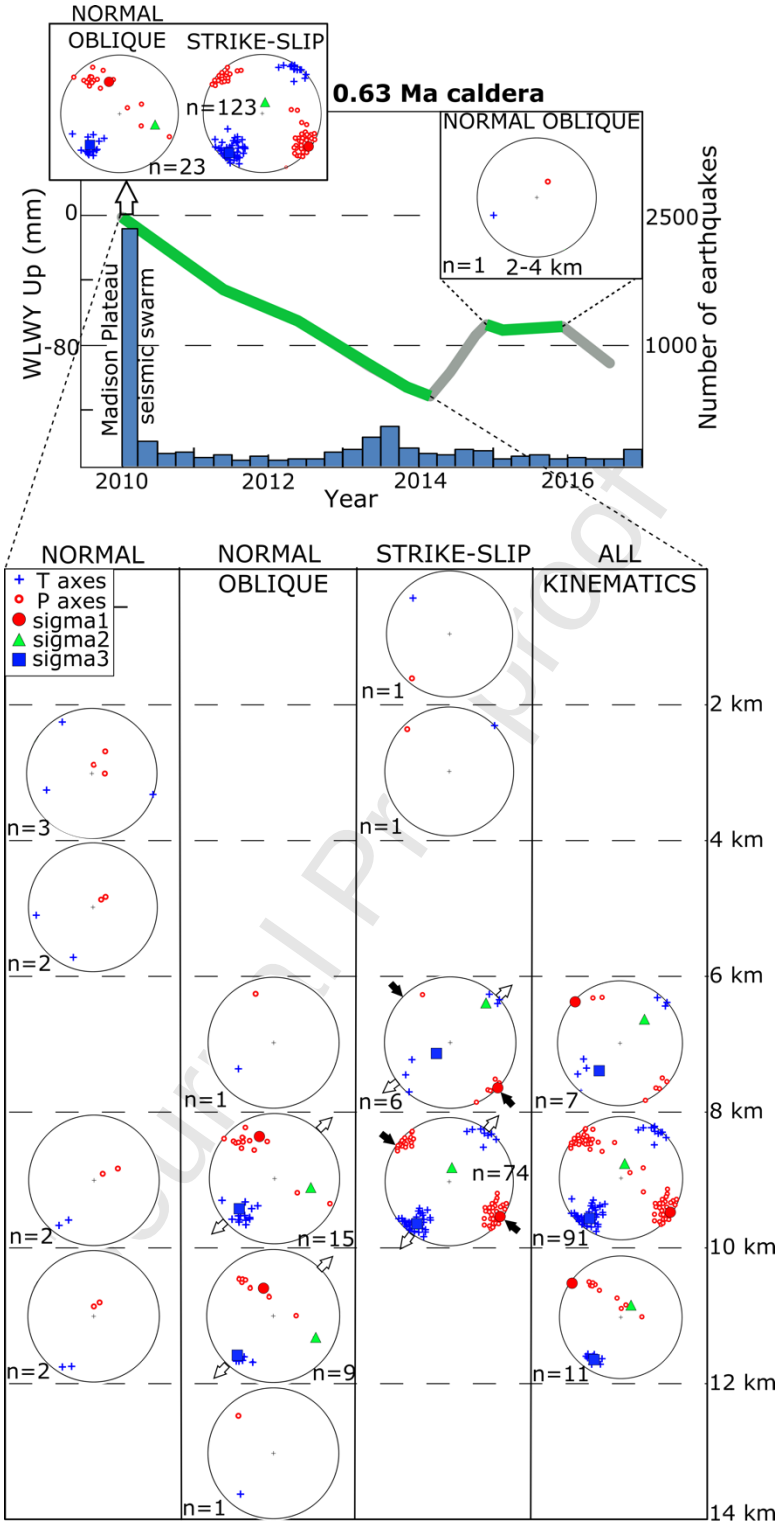

Figure 8: *Seismic events of the inner part of the 0.63 Ma Yellowstone caldera (119 selected earthquakes) divided into kinematics, depth and temporal windows, according to phases of surficial deformation recorded at WLWY GPS station between 2010 and 2016. P and T axes are represented as red circles and blue crosses respectively, the orientation of principal stress axis (when calculated) is indicated as red circles for σ_1, green triangles for σ_2 and blue squares for σ_3.*

Diverging white arrows indicate direction of extension (σ_3), converging black arrows direction of compression (σ_1). Earthquake occurrence rate, considering relocated hypocenters of our database, divided per quarter of year, is shown in the graph.

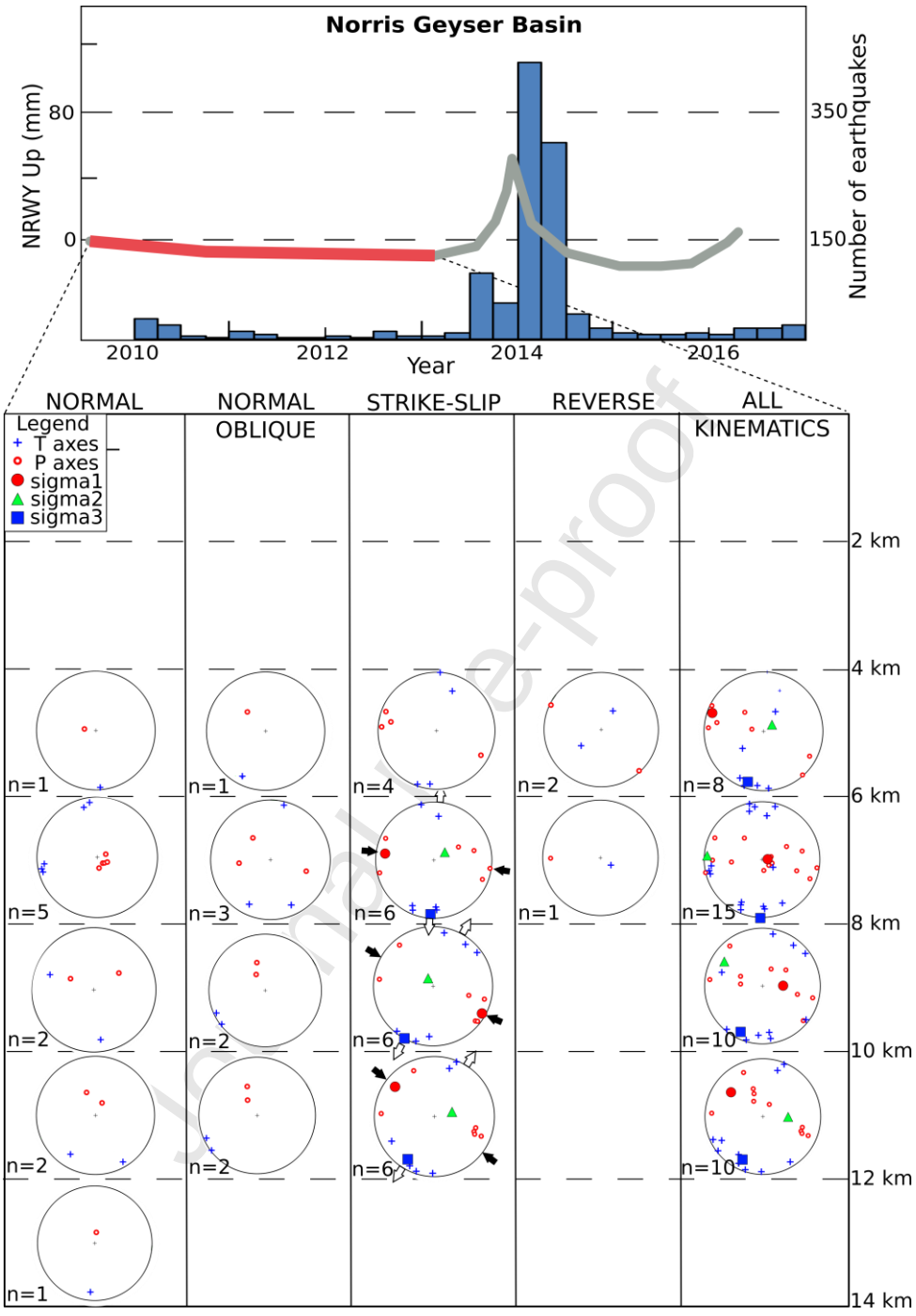

Figure 9: *Seismic events of the outer part of the 0.63 Ma Yellowstone caldera, in the Norris Geyser Basin area (44 selected earthquakes), divided into kinematics, depth and temporal windows, according to phases of surficial deformation recorded at NRWY GPS station between 2010 and 2013. P and T axes are represented as red circles and blue crosses respectively, the orientation of principal stress axis (when calculated) is indicated as red circles for* sigma$_1$*, green*

triangles for sigma$_2$ *and blue squares for* sigma$_3$*. Diverging white arrows indicate direction of extension (*sigma$_3$*), converging black arrows direction of compression (*sigma$_1$*). Earthquake occurrence rate, considering relocated hypocenters of our database, divided per quarter of year is shown in the graph.*

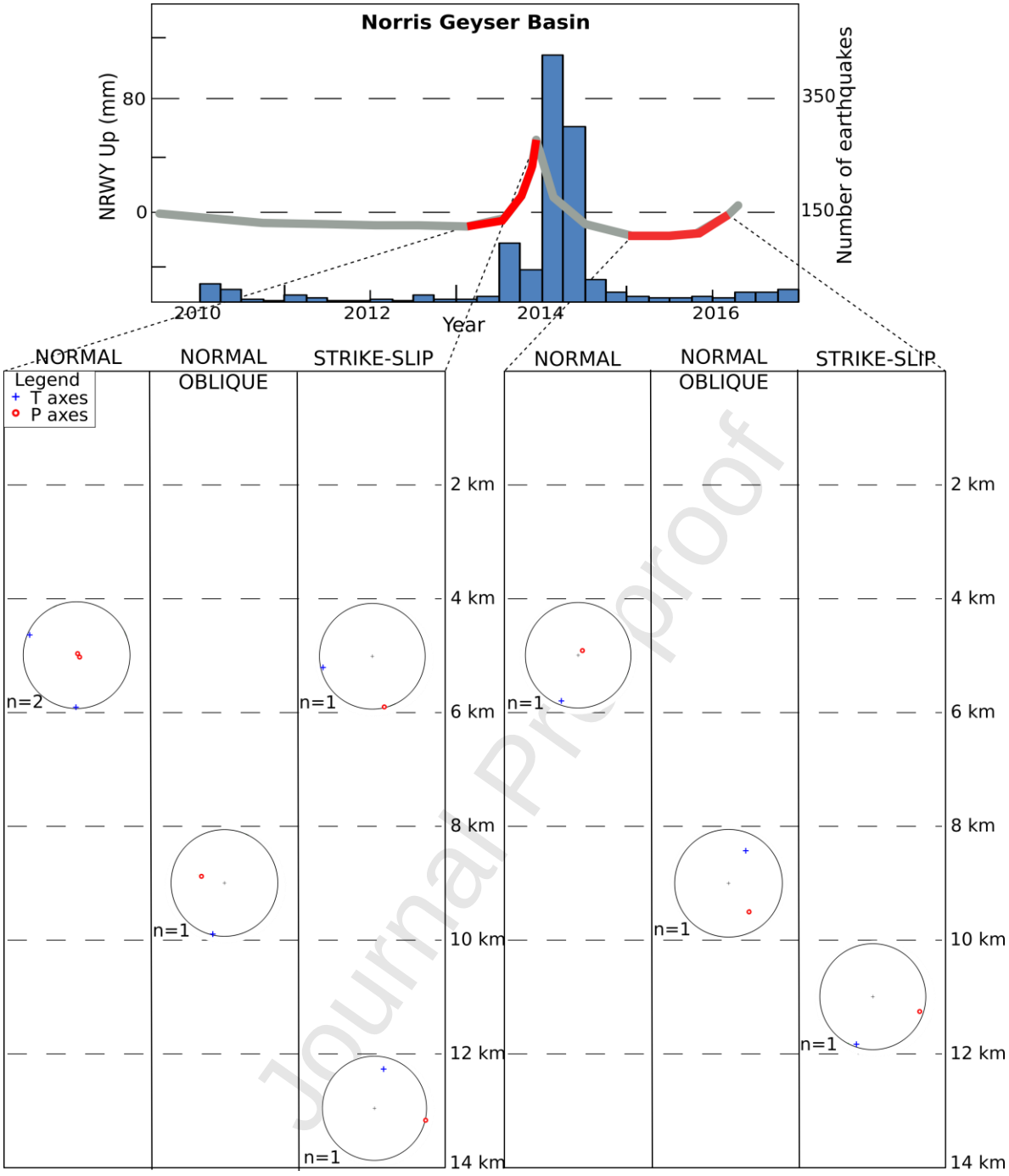

Figure 10: *P and T axes calculations of the outer part of the 0.63 Ma Yellowstone caldera, in the Norris Geyser Basin area (7 selected earthquakes), divided into kinematic, depth and temporal windows, according to phases of surficial deformation recorded at NRWY GPS station between 2013 and 2014, and 2015 and 2016. P and T axes are represented as red circles and blue cross respectively. Earthquake occurrence rate, considering relocated hypocenters of our database, divided per quarter of year is shown in the graph.*

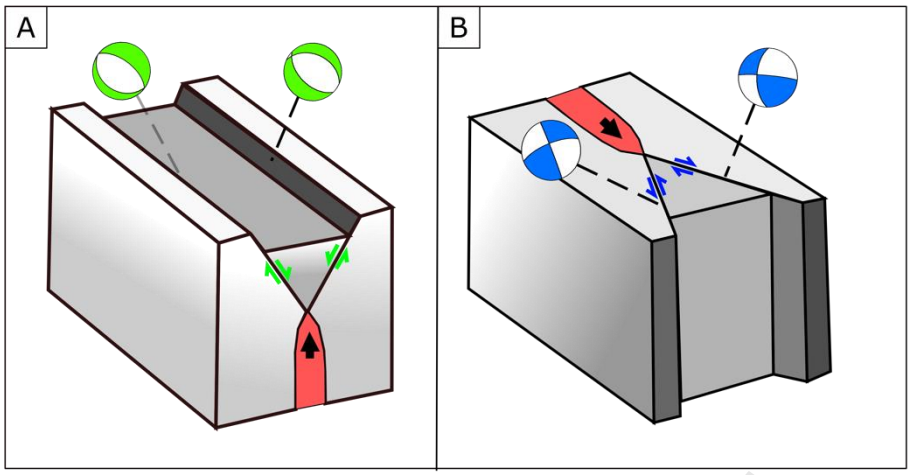

Figure 11. *Geomechanical model of brittle deformations resulting from the stress field linked to the propagation of fluids in different directions: A) refers to upward propagation of magma, and B) to horizontal magma propagation along vertical planes. The beach balls give the typical kinematics revealed by the FMS calculated in this work for Yellowstone (green = normal faulting, blue = strike-slip faulting). The red zone gives the plane from which magmatic fluids propagate and the black arrow shows the fluid flow direction.*

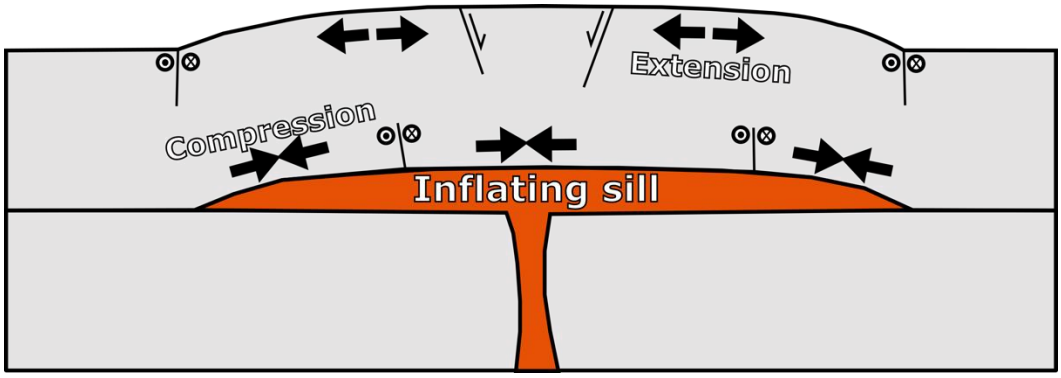

***Figure 12**: Geomechanical model of brittle deformation above an inflating sill and in the surroundings. Circles define motion of strike-slip faults. Diverging arrows show extension in the extrados zone of the upwarping overburden, converging arrows show compression in the intrados zone.*

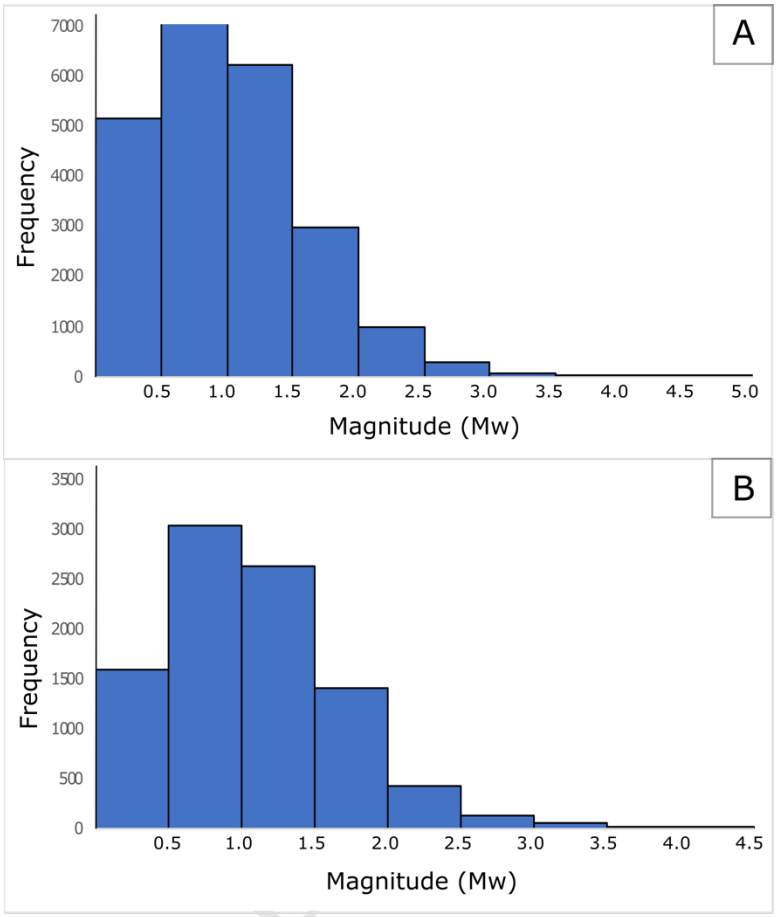

Figure 13. *Graph showing magnitude of seismic events vs. frequency for the period 1988-2009 (A) and 2010-2016 (B).*

Quality	Average misfit	RMS fault plane uncertainty	Station distribution ratio	Mechanism probability
A	≤ 0.15	≤ 25°	≥ 0.5	≥ 0.8
B	≤ 0.20	≤ 35°	≥ 0.4	≥ 0.6
C	≤ 0.30	≤ 45°	≥ 0.3	≥ 0.7
D	maximum azimuthal gap ≤ 90°, maximum takeoff angle gap ≤ 60°			
E	maximum azimuthal gap > 90°, maximum takeoff angle gap > 60°			
F	fewer than 8 polarities			

***Table 1**: Focal mechanism quality determination (modified after Hardebeck and Shearer, 2002).*

HIGHLIGHTS

224 new double-couple focal mechanism solutions have been computed at Yellowstone
Most give strike-slip faulting, with subordinate normal and a few reverse motions
Fault kinematics have been compared with magma inflation and deflation phases
The causes of dominant horizontal fluid migration are discussed